Self-consistent modelling study on discharge poisoning

Santu Luo[1], Dingxin Liu[1], Wang Xi[1] and Mingzhe Rong[1]

[1]*Center for Plasma Biomedicine, Xi'an Jiaotong University, Xi'an, Shaanxi 710049, China*

Abstract: Discharge poisoning has been a century-old problem of air plasma and gained new importance in recent years due to the development of such plasma in biomedicine and nitrogen fixation. Here, a kinetic model is developed which newly incorporates tens of vibrational excited species and some decomposition reactions of N_2O_5, and hence it for the first time reproduces the experimental results of discharge poisoning self-consistently. The mechanism of discharge poisoning is then elucidated systematically in quantitative level.

Keywords: Discharge poisoning, kinetic model, rective species, transition state theory

1. Introduction

Air discharge plasma is the main method of O_3 production in industry, but when the discharge power and/or the gas temperature exceeds a certain level, nearly no O_3 is formed anymore which is referred as "discharge poisoning" [1, 2]. Discharge poisoning is the bottleneck limiting the yield of ozone generators, but in turn it expands the use of air discharge plasma to new application fields such as nitrogen fixation, because in that case the main products are NO and/or NO_2 [3, 4]. Although the discovery of discharge poisoning date back more than 100 years ago [5, 6], the underlying mechanism is still not well understood, as reflected by the fact that there is no numerical model in the literature which could simulate the discharge poisoning self-consistently. The discharge poisoning is a key problem in plasma science, and technologically it is a major hinderance for air discharge plasma to be developed in environmental protection, chemical engineering, biomedical applications and so on. In view of this, the discharge poisoning was investigated in this paper by means of simulation and experiments.

2. Kinetic model and experiments

A surface dielectric barrier discharge (SDBD) reactor was used for generating air plasma in a shielded gas chamber, which has been reported previously [7]. The size of surface plasma was 5 cm × 5 cm and the height of the gas chamber was 4 cm. The plasma-generated reactive species in the gas chamber was detected by a FTIR (Bruker, TensorII), of which the vibrational bands of 2235 cm^{-1}, 1900 cm^{-1}, 1630 cm^{-1}, 1720 cm^{-1} and 1055 cm^{-1} were employed for the detection of N_2O, NO, NO_2, N_2O_5 and O_3, respectively [8]. The discharge power (P_d) and gas temperature (T_g) were both controllable, and discharge poisoning could be ignited with the increase of either discharge power or gas temperature.

The simulation model was developed according to the experimental setup, which consisted of two modules, i.e. a plasma module for the surface plasma and a diffusion module for the afterglow region in the chamber. The densities of reactive species were assumed homogeneous in either the plasma or the afterglow region, with the particle balance equations as follow:

$$\frac{\partial n_p}{\partial t} = \sum_j k_j \prod n_{p,j} - \frac{r \cdot \Gamma_{pg}}{d_p} \quad (1)$$

$$\frac{\partial n_g}{\partial t} = \sum_j k_j \prod n_{g,j} + \frac{\Gamma_{pg}}{r \cdot d_g} \quad (2)$$

$$\Gamma_{pg} = \frac{D(n_p - n_g)}{0.5(d_p + d_g)} \quad (3)$$

Where n_g, n_p represent the density of reactive species in plasma region and diffusion region respectively. k_j is the reaction coefficient of considered reations, Γ_{pg} is the flux between plasma and the diffusion region, D is the diffusion coefficient, d_p and d_g are the thickness of considered regions, r is a factor accounting for the axial diffusion of reactive species.

The simulation model was developed based on a plasma-liquid model as reported previously [9]. In comparsion, the liquid phase was deleted, and the reaction kinetics in the gas phase was modified to better describe the production/reduction of key species including O_3, NO, N_2O_5 which are responsible for discharge poisoning. Vibrational excited N_2 and O_2 are believed to be effective in producing NO which consequently suppresses the O_3 accumulation [10]. Hence, the vibrational kinetics of N_2 and O_2 including the eletron impact reactions, vibrational-vibrational (VV) relaxation reactions and vibrational-transitional (VT) relaxation reactions were incorporated in the model. Besides, the vibrational excited NO_2 and O_3 (only asymmetric stretching mode) were also added in the model because they couldn quench O atoms [11,12]. The rate constants of the reactions between vibrational excited molecules and other reactive species were calculated by Fridman approxiamation [13] or gathered from literatures [14,15]. In addition, the removal reaction of N_2O_5 was only thermal decomposition in the reported model [9], and consequently the density of N_2O_5 was too high. However, other removal reactions of N_2O_5 were not reported in the literature. In view of this, the combination of transition state theory and density functional theory were employed to calculate the reaction rates between N_2O_5 and other reactive species. It was found that the N_2O_5 had strong reactions with NO and O, of which the rate coefficients were $1.63\times10^{-7}\exp(-21225/T_g)$ and $2.54\times10^{-7}\exp(-2762.81/T_g)$ $cm^3\cdot s^{-1}$, respectively. The calculated energy profiles of the N_2O_5-involved reactions were shown in Fig. 1, and our calculation is also a supplement to the Wilson's work [16].

In the model, 60 reactive species and 864 reactions were involved in the plasma module, while 34 neutral species and 352 species were involved in the diffusion module. All the reactions were calculated using the differential equation solvers intergrated in COMSOL Multiphysics® software.

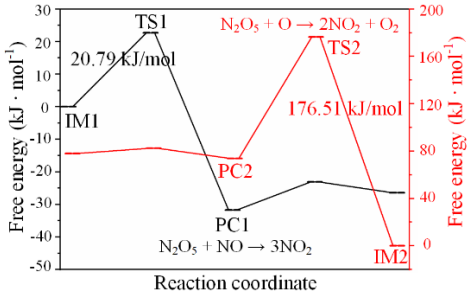

Fig. 1 Potential energy surface of calculated reactions for N_2O_5 reduction

3. Results and disscussion

When the discharge power is 3 W and the gas temperature is 25 ℃, experimental and simulation results show that the plasma operates in ozone mode, i.e. the main reaction species is O_3 with a high density of ~200 ppm, but the density of other species including NO, NO_2 are negligible. This means that discharge poisoning does not happen in the condition. However, when the discharge power increases to 6 W (the gas temperature stays at 25 ℃), discharge poisoning happens as illustrated in Fig. 2. It should be noted that the points are experimental results and the curves are simulation results, indicating that the simulation could reproduce the experiments in quantitative level. According to the experimental results, O_3 is the dominant reactive species in the beginning 100 seconds. It accumulates to a peak value of ~100 ppm at the time of 50 s and then drops to less than 1 ppm at the time of 150 s. Similarly, the density of N_2O_5 increases to a peak value of 50 ppm at the time of 75 s and then decreases to less than 1 ppm at the time of 150 s. After that, NO and NO_2 become the dominant species and O_3 and N_2O_5 could not be detected, indicating that the discharge is poisoned. The density of NO_2 is low at beginning of the discharge, but it increases exponentially in the first 150 s to a high value of ~320 ppm, and then the increase trend becomes linearly. Interestingly, the density of NO is detectable when N_2O_5 is nearly disappear, suggesting that there should be strong reaction between the two species, and after that it increases linearly to ~90 ppm at the discharge time of 300 s.

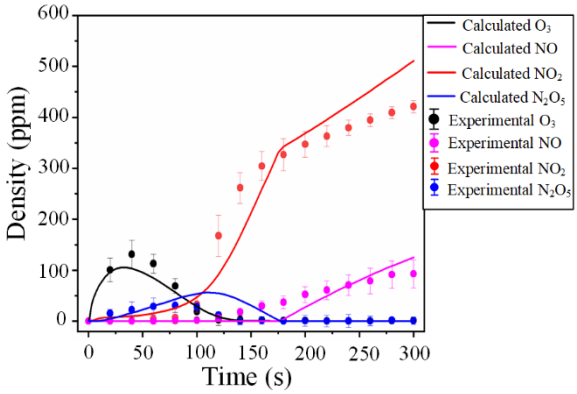

Fig. 2 Density variation of reactive species with the discharge time (P_d=6 W, T_g=25 ℃)

Discharge poisoning also happens when the discharge power is 3 W and the gas temperature is increased to 100 ℃, as shown in Fig. 3. In this condtion, the simulation also reproduces the experiments well although the density error is comparatively larger. According to the experimental results, the density of O_3 increases at beginning and reaches a peak value of 50 ppm at the time of 25 s, then it drops sharply to blow 1 ppm within 100 s. The density of N_2O_5 reaches its peak value of 30 ppm at the time of 80 s and falls below 1 ppm at 180 s. NO_2 is detectable when the density of O_3 is less than 10 ppm, and then it accumulates continuously to ~500 ppm at the time of 300 s. NO is detectable when the density of N_2O_5 is very low, and then it increases linearly to ~100 ppm at the time of 300 s. Compared to the condition shown Fig. 2, the discharge poisoning in this condition happens faster so that the peak densities of O_3 and N_2O_5 are lower.

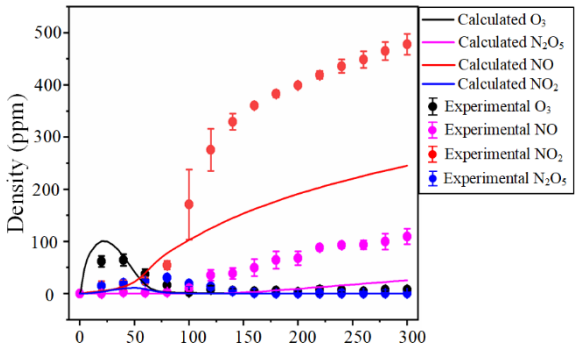

Fig. 3 Density variation of reactive species with the discharge time (P_d=3 W, T_g=100 ℃)

Discharge poisoning should be attributed to 1) the drop of O_3 generation rate and 2) the increase of O_3 quenching rate. To inlustrate the underlying mechanism of discharge poisoning, the yields and consumption of main reactions for O_3 are shown in Fig. 4, as a function of the discharge time. This result is for the condition of P_d=6 W and T_g=25 ℃, and that for another condition of P_d=3 W and T_g=100 ℃ is not plotted here because the results are similar.

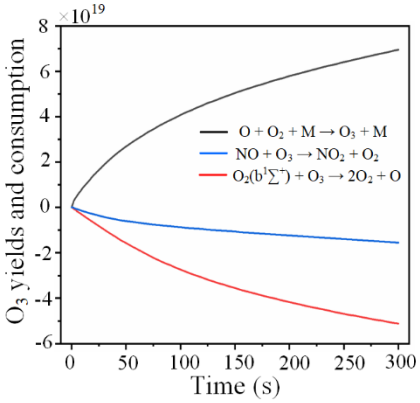

Fig. 4 The yields and consumption of main reactions for O_3 with the discharge time (P_d=6 W, T_g=25 ℃)

As shown in Fig. 4, the main generation reaction of O_3 is the three-body reaction (4), which contributes to 99% yields of O_3. It can be seen that the reaction rate of (4) is

decreasing with the discharge time, indicating that the density of O atoms is decreasing.

$$O + O_2 + M \rightarrow O_3 + M \quad (4)$$

O_3 is mainly consumed by reaction (5) and (6). Nearly 80% of O_3 are consumed by reaction (5) in which $O_2(b^1\sum^+)$ is produced by the electron impact exciation of O_2, so the consumption rate of O_3 increases with the electron density and further the discharge power. However, more O is produced when the discharge power is increased, so the production rate of O_3 also increases by reaction (4), suggesting that the reactions (4) and (5) do not play a key role in discharge poisoning. Reaction (6) is a main link between O_3 and NO/NO_2 which should be important for discharge poisoning, and the yields and consumption of NO are ploted in Fig. 5.

$$O_2(b^1\sum^+) + O_3 \rightarrow 2O_2 + O \quad (5)$$

$$NO + O_3 \rightarrow NO_2 + O_2 \quad (6)$$

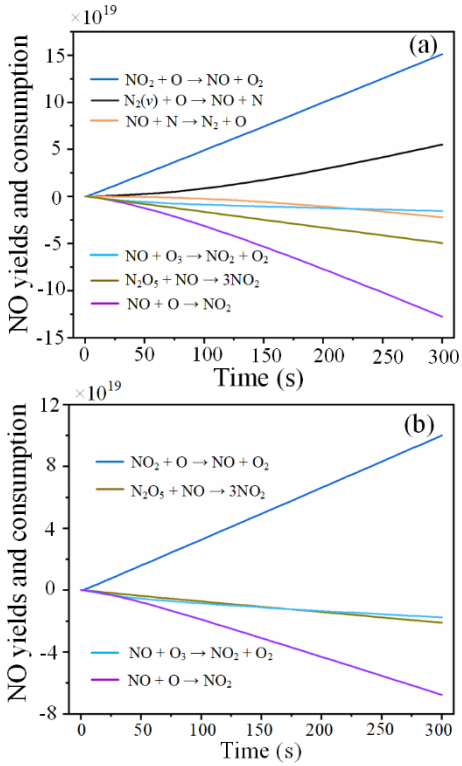

Fig. 5 The yields and consumption of main reactions for NO with the discharge time. (a) P_d=6 W, T_g=25 ℃; (b) P_d=3 W, T_g=100 ℃

When the discharge power is 6 W and the gas temperature is 25 ℃, nearly 80% of NO is generated by reaction (7) and consumed by reaction (8). These two reactions constitutes a catalysis recombination cycle, i.e. NO and NO_2 are not consumed because when the reactant contains one, the product contains the other. Another main generation reaction of NO is reaction (9), which contributes to almost 95% net production of NO. Besides the reaction (8), nearly 20% NO is consumed through the reaction (10) to form NO_2, which has never been considered in the literature. Moreover, given the catalystic recombination cycle of the reaction (7) and (8), the reaction (10) contributes to more than 50% net consumption of NO.

$$NO_2 + O \rightarrow NO + O_2 \quad (7)$$

$$NO + O \rightarrow NO_2 \quad (8)$$

$$N_2(v) + O \rightarrow NO + N \quad (9)$$

$$N_2O_5 + NO \rightarrow 3NO_2 \quad (10)$$

When the discharge power is 3 W and gas temperature is 100 ℃, the total generation of NO through reaction (7) and consumption through reaction (8) are not matched. The reaction (7) generates more NO than the reaction (8) consumes, indicating that density ratio of NO_2 and NO is higher. The reaction (7) contributes nearly 90% net generation of NO, while the reaction (9) only contributes 5% net generation of NO, suggesting that the temperature rise has little effect on the production of $N_2(v)$. Therefore, the discharge poisoning ignited by the rise in gas temperature should not be attributed to the vibrational excitation reactions. Also, the contribution of N_2O_5 on the consumption of NO is reduced, because the reactions for N_2O_5 production is very sensitive to the gas temperature.

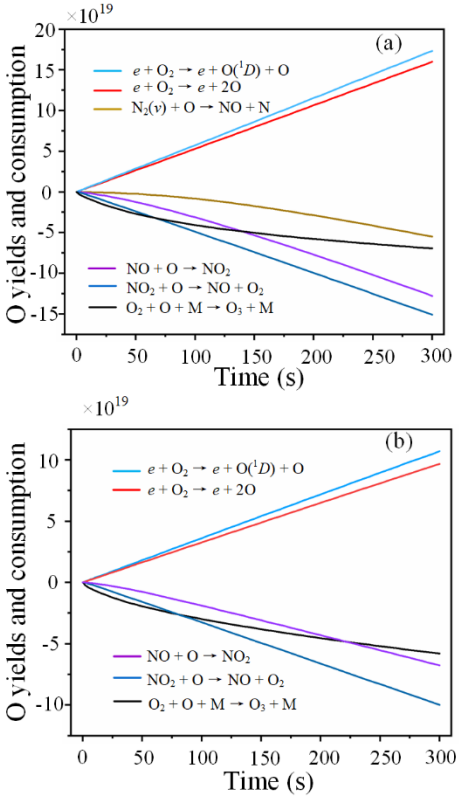

Fig. 6 The yields and consumption of main reactions for O with the discharge time. (a) P_d=6 W, T_g=25 ℃; (b) P_d=3 W, T_g=100 ℃

Fig. 6 illustrates the time-dependent O yieds and consumption for the two conditions. The atomic oxygen is mainly generated by electron impact dissociation, so increasing discharge power rather than gas temperature could enhance the production. However, the increase in discharge power also lead to higher densities of NO and NO_2 and consequently more O is consumed by reaction (7) and (8). Besides, more $N_2(v)$ is produced which plays an important role in the consumption of O. As a result, the yields of O_3 by reaction (4) is almost the same for the two conditions (see the black curves in the Fig. 4). The discharge poisoning phenomenon ignited by the increase of discharge power is usually similar to that ignited by the increase of gas temperature, however, the results suggest that the underlying mechanism should be much different.

In conclusion, a self-consistent model for air discharge plasma and its afterglow region was developed, and it for the first time reproduced the experimental results of discharge poisoning process in quantitative level. Besides the catalystic recombination cycle of NO and NO_2 which has been reported to play a key role in discharge poisoning, it is found that $N_2(v)$ is also important for the discharge poisoning ignited by increasing discharge power, while N_2O_5 plays an important role for the discharge poisoning ignited by increasing gas temperature.

4. Acknowledgment

This work was supported by the National Science Foundation of China (Grant No. 52150221), and the State Key Laboratory of Electrical Insulation and Power Equipment (EIPE22122).

5. References

[1] B. Eliasson et al. IEEE Trans. Plasma Sci. 19(2): 309-323 (1992).
[2] B. Eliasson and U. Kogelschatz, Proc. 8th Int. Symp. Plasma Chem. (ISPC-8), Tokyo (1987).
[3] J. G. Chen, et al. Science, 360: 873 (2018).
[4] L. R.Winter and J. G. Chen, Joule, 5(2): 300-315 (2021).
[5] E.Warburg and G. Leithäuser, Annalen der Physik, 325.9: 751-758 (1906).
[6] A. Thomas and P. G. Tait. Philosophical Transactions of the Royal Society of London, 150: 113-131 (1860).
[7] W. Xi et al, Plasma Sources Sci. Technol. 29: 095013 (2020).
[8] M. J. Pavlovich, et al, J. Phys. D: Appl. Phys. 46: 145202 (2013).
[9] Z. C. Liu, et al. J. Phys. D: Appl. Phys. 48: 495201 (2015).
[10] T. Shimizu, et al. New J. Phys., 14: 103028 (2012).
[11] W. T. Rawlins, J. Geophys. Research, 90(12): 12283-12292 (1985).
[12] B Eliasson, et al. J. Phys. D: Appl. Phys., 20: 1421-1437 (1987).
[13] A. Fridman. Plasma chemistry. Cambridge university press (2008).
[14] W. T. Rawlins and G. E. Caledonia, J. Chem. Phys. 87: 5209 (1987).
[15] J. A. Joens, et al. J. Chem. Phys. 76: 5902 (1982).
[16] D. J. Wilson and H. S. Johnston, J. Am. Chem. Soc., 75(22): 5763 (1953).